

Crystal structure and characterization of the sulfamethazine–piperidine salt

Juan Saulo González-González,^{a*} Salvador Pérez-Espinoza,^a Francisco Javier Martínez-Martínez,^b Armando Pineda-Contreras,^b Miguel Ángel Canseco-Martínez,^c Marcos Flores-Alamo^d and Héctor García-Ortega^{d*}

Received 10 November 2022

Accepted 21 December 2022

Edited by I. Oswald, University of Strathclyde, United Kingdom

Keywords: sulfamethazine; piperidine; IR spectroscopy; crystal structure; solid-state ¹³C NMR; thermal analysis; proton transfer; solvent-assisted grinding.

CCDC reference: 2214090

Supporting information: this article has supporting information at journals.iucr.org/c

^aInstituto de Farmacobiología, Universidad de la Cañada, Carretera Teotitlán-San Antonio Nanahuatipán, km 1.7 s/n, Teotitlán de Flores Magón, Oaxaca, 68540, Mexico, ^bFacultad de Ciencias Químicas, Universidad de Colima, km 9 Carretera Colima-Coquimatlán, Coquimatlán, Colima, 28400, Mexico, ^cInstituto de Investigación en Materiales, Universidad Nacional Autónoma de México, Ciudad de México, 04510, Mexico, and ^dFacultad de Química, Universidad Nacional Autónoma de México, 04510, Ciudad de México, Mexico. *Correspondence e-mail: juan_saulo@unca.edu.mx, hector.garcia@unam.mx

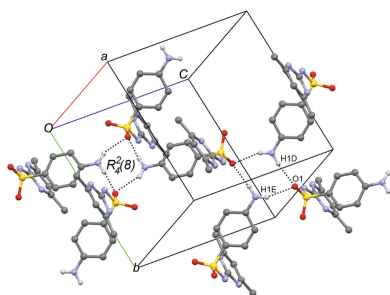
Sulfamethazine [*N*¹-(4,6-dimethylpyrimidin-2-yl)sulfanilamide] is an antimicrobial drug that possesses functional groups capable of acting as hydrogen-bond donors and acceptors, which make it a suitable supramolecular building block for the formation of cocrystals and salts. We report here the crystal structure and solid-state characterization of the 1:1 salt piperidinium sulfamethazinate (PPD⁺–SUL[−], C₅H₁₂N⁺·C₁₂H₁₃N₄O₂S[−]) (**I**). The salt was obtained by the solvent-assisted grinding method and was characterized by IR spectroscopy, powder X-ray diffraction, solid-state ¹³C NMR spectroscopy and thermal analysis [differential scanning calorimetry (DSC) and thermogravimetric analysis (TGA)]. Salt **I** crystallized in the monoclinic space group *P*2₁/*n* and showed a 1:1 stoichiometry revealing proton transfer from SUL to PPD to form salt **I**. The PPD⁺ and SUL[−] ions are connected by N–H⁺⋯O and N–H⁺⋯N interactions. The self-assembly of SUL[−] anions displays the amine–sulfa *C*(8) motif. The supramolecular architecture of salt **I** revealed the formation of interconnected supramolecular sheets.

1. Introduction

Sulfonamides are antimicrobial drugs used for the treatment of human and veterinary bacterial infections, and act by inhibiting the enzyme dihydropteroate synthase, a key enzyme involved in folate synthesis (Ovung & Bhattacharyya, 2021). The chemical structure of sulfonamides includes SO₂, NH and NH₂ groups capable of acting as hydrogen-bond donors and acceptors, and also arene rings capable of forming π -interactions, which make them suitable supramolecular building blocks for use in crystal engineering for the formation of pharmaceutical cocrystals (Caira, 2007).

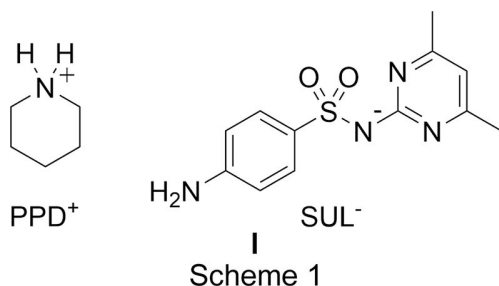
Pharmaceutical cocrystals are crystalline materials composed of an active pharmaceutical ingredient (API) and a cocrystal coformer which remain together in the crystalline lattice principally *via* hydrogen-bond interactions. Pharmaceutical cocrystallization offers the possibility of obtaining new solid forms of APIs and improving poor physicochemical properties (Bolla & Nangia, 2016).

Sulfamethazine (SUL) cocrystals, solvates and salts have been prepared to study its ability to form noncovalent interactions, amidine–imidine tautomerism and proton transfer (Ghosh *et al.*, 2011; Zhang *et al.*, 2017; Singh & Baruah, 2019). Concerning the improvement of physicochemical and pharmaceutical properties, cocrystals of sulfamethazine with



4-aminosalicylic acid and 4-aminobenzoic acid enhance solubility, dissolution and antibacterial activity (Pan *et al.*, 2019; Serrano *et al.*, 2016).

Piperidine (PPD) is a heterocyclic amine that possesses an N–H group able to act as a hydrogen-bond donor. Combination with pharmaceutical ingredients gives rise to the formation of cocrystals (with curcumin; Sanphui & Bolla, 2018) or salts [with diclofenac (Fini *et al.* 2012) and sulfapyridine (Pratt *et al.*, 2011)]. The formation of cocrystals or



salts can be predicted (not exactly) using the ΔpK_a criteria from $[pK_a(\text{base}) - pK_a(\text{acid})]$. When the value of ΔpK_a is greater than 3, salt formation occurs, and when the value of ΔpK_a is less than 0, cocrystal formation occurs. ΔpK_a values between 0 and 3 do not give clear information about the cocrystal/salt preference (Kumar & Nanda, 2018). We report here a crystallization study between sulfamethazine ($pK_a = 7.40$; Zhang *et al.*, 2016) and piperidine ($pK_a = 11.10$; Luna *et al.*, 2016) (Fig. 1), producing the $\text{PPD}^+\cdot\text{SUL}^-$ salt, **I** ($\Delta pK_a = 3.7$) (Scheme 1) by solvent-assisted grinding and solvent evaporation. The solid-state characterization was performed by IR spectroscopy (IR), powder X-ray diffraction (PXRD), solid-state nuclear magnetic resonance (^{13}C NMR) spectroscopy, differential scanning calorimetry (DSC) and thermogravimetric analysis (TGA). The crystal structure was obtained by single-crystal X-ray diffraction.

2. Experimental

2.1. Synthesis and crystallization

Sulfamethazine and piperidine were purchased from Aldrich. Dichloromethane and ethanol were purchased from Química Mayer. All reagents were used as received.

Sulfamethazine (0.3 g, 1.077 mmol) and piperidine (0.106 ml, 1.077 mmol), in a 1:1 molar ratio, were placed in a mortar. Before grinding, 0.5 ml of dichloromethane was added. The mixture was then ground with a pestle for 3 min. After the grinding time, the dichloromethane was evaporated and the powder was collected in the centre of the mortar. The cycle of adding 0.5 ml of dichloromethane and grinding for 3 min was repeated three more times until a grinding time of 12 min was reached. The polycrystalline ground powder of **I** was collected and stored in a glass vial. Single crystals suitable for X-ray diffraction were obtained from a solution of **I** in ethanol left to evaporate at room temperature.

2.2. IR spectroscopy

The IR spectra of solid powders of SUL and PPD, the polycrystalline powder of **I** and the single crystal of **I** were acquired in a Bruker Tensor 27 spectrophotometer equipped with an attenuated total reflectance (ATR) system accessory (16 scans, spectral range 600–4000 cm^{-1} , resolution 4 cm^{-1}).

2.3. Powder X-ray diffraction

Powder X-ray diffraction (PXRD) patterns of SUL, PPD and the polycrystalline powder of **I** were recorded on a PANalytical X'Pert PRO diffractometer with $\text{Cu } K\alpha_1$ radiation ($\lambda = 1.5405 \text{ \AA}$, 45 kV, 40 mA) from 2.02 to 49.93° in 2θ .

2.4. Solid-state ^{13}C NMR

Cross-polarization/magic angle spinning (CP/MAS) ^{13}C NMR experiments of the solid powders of SUL and the polycrystalline powder of **I** were performed on a Bruker 400 Avance III (^{13}C , 100 MHz) instrument at 25 °C. 4 mm bullet-type Kel-F zirconia rotors were used (containing about 100 mg of the sample). The spinning rate and acquisition time were 8 kHz and 32 ms, respectively. The recycle time of the pulse was 3 s. The adamantane signal was used as the external reference ($\delta = 38.48 \text{ ppm}$).

2.5. Thermal analysis

Differential scanning calorimetry (DSC) measurements were obtained on a TA Instruments Q100 instrument. Samples placed in aluminium pans were heated from 25 to 255 °C under a nitrogen atmosphere at a rate of 10 °C min^{-1} . Thermogravimetric analysis (TGA) was performed on a TA Instruments SDT Q600 instrument. Samples placed in aluminium pans were heated from 25 to 315 °C under a nitrogen atmosphere at a rate of 10 °C min^{-1} . Heating of **I** was performed in a VelaQuin 9053A oven at 185 °C for 1 h (arbitrary time).

2.6. Refinement

Crystal data, data collection and structure refinement details are summarized in Table 1. The H atoms of amine N–H groups were located in a difference map and refined isotropically with $U_{\text{iso}}(\text{H}) = 1.2U_{\text{eq}}(\text{N})$. H atoms attached to C atoms were placed in geometrically idealized positions and refined as riding on their parent atoms, with C–H = 0.95–0.99 Å and $U_{\text{iso}}(\text{H}) = 1.2U_{\text{eq}}(\text{C})$ for aromatic and methylene groups, and $1.5U_{\text{eq}}(\text{C})$ for methyl groups.

3. Results and discussion

3.1. Solid-state characterization of salt **I**

The formation of the new solid phase of salt **I** was evidenced by IR spectroscopy because the IR spectrum was different from those of the starting materials PPD and SUL, showing shifts in the N–H and SO_2 bands (Fig. 1), indicating the formation of intermolecular interactions [the IR spectra of SUL and PPD were assigned according with Yang *et al.* (2005)

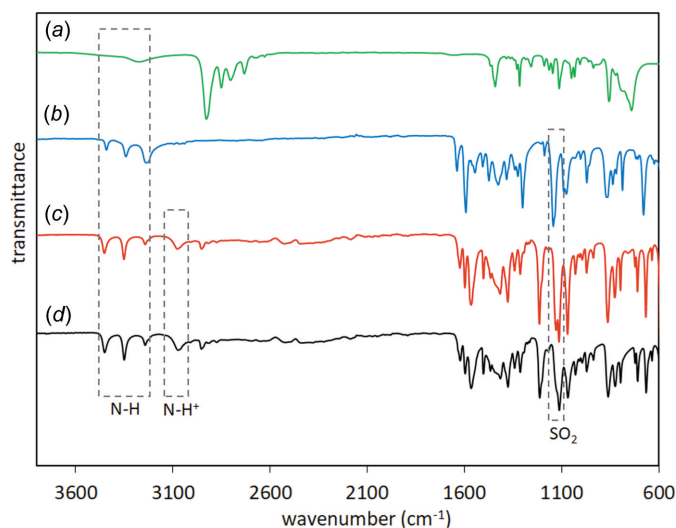


Figure 1
IR spectra of (a) PPD, (b) SUL, (c) the polycrystalline powder of **I** and (d) crystal **I**.

and Güllüoğlu *et al.* (2007), respectively]. The distinctive bands in the IR spectra of the polycrystalline powder of **I** and the single crystal of **I** are those at 3076 and 3073 cm^{-1} , respectively, belonging to the piperidinium N—H⁺ group (Silverstein *et al.*, 1991); also, the SO₂ band at 1114 cm^{-1} in the polycrystalline powder and the single crystal of **I**, which is shifted to a lower wavenumber with respect to the starting material SUL (1145 cm^{-1}), indicated deprotonation of the sulfonamide group, as observed in the formation of the benzamidinium sulfamerazinate salt (Kamali *et al.*, 2015) and in the formation of metallic complexes of SUL with silver and copper (Tailor & Patel, 2015). The N—H bands of SUL were also shifted from 3441 and 3339 to 3452 and 3351 cm^{-1} in the polycrystalline powder of **I**, and to 3451 and 3350 cm^{-1} in the single crystal of **I** (Fig. 1).

The experimental PXRD pattern of SUL matched well with the simulated pattern obtained from *Mercury* (Macrae *et al.*,

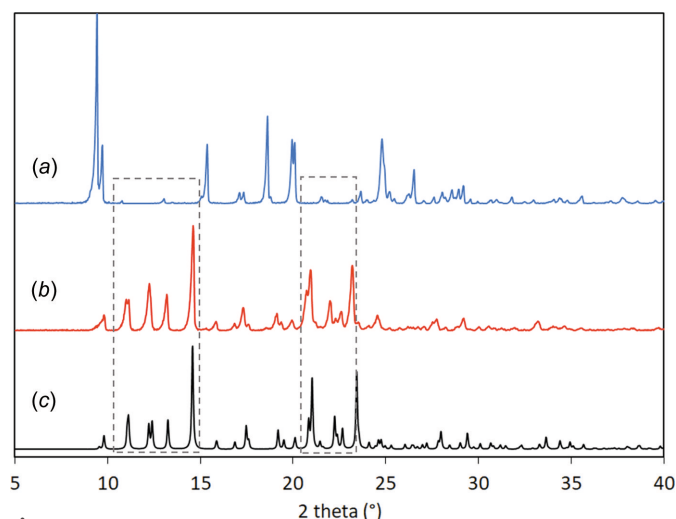


Figure 2
Powder X-ray diffractograms of (a) SUL, (b) the polycrystalline powder of **I** and (c) the simulated pattern for **I**.

Table 1
Experimental details.

Crystal data	
Chemical formula	C ₅ H ₁₂ N ⁺ ·C ₁₂ H ₁₃ N ₄ O ₂ S ⁻
<i>M_r</i>	363.48
Crystal system, space group	Monoclinic, <i>P</i> 2 ₁ / <i>n</i>
Temperature (K)	130
<i>a</i> , <i>b</i> , <i>c</i> (Å)	10.5713 (7), 12.1313 (8), 14.3623 (10)
β (°)	97.182 (7)
<i>V</i> (Å ³)	1827.4 (2)
<i>Z</i>	4
Radiation type	Mo <i>K</i> α
μ (mm ⁻¹)	0.20
Crystal size (mm)	0.53 × 0.43 × 0.34
Data collection	
Diffractometer	Agilent Xcalibur Atlas Gemini
Absorption correction	Analytical (<i>CrysAlis PRO</i> ; Agilent, 2013)
<i>T_{min}</i> , <i>T_{max}</i>	0.93, 0.945
No. of measured, independent and observed [<i>I</i> > 2 σ (<i>I</i>)] reflections	10086, 4298, 3667
<i>R_{int}</i>	0.025
Refinement	
<i>R</i> [<i>F</i> ² > 2 σ (<i>F</i> ²)], <i>wR</i> (<i>F</i> ²), <i>S</i>	0.037, 0.102, 1.04
No. of reflections	4298
No. of parameters	241
H-atom treatment	H atoms treated by a mixture of independent and constrained refinement
$\Delta\rho_{\text{max}}$, $\Delta\rho_{\text{min}}$ (e Å ⁻³)	0.37, -0.44

Computer programs: *CrysAlis PRO* (Agilent, 2013), *SHELXT2018* (Sheldrick, 2015a), *SHELXL2018* (Sheldrick, 2015b) and *ORTEP* for Windows (Farrugia, 2012).

2020) for the Cambridge Structural Database (CSD; Groom *et al.*, 2016) refcode SLFNMD01 (Basak *et al.*, 1983). The PXRD pattern of the polycrystalline powder of **I** was different from the PXRD pattern of SUL and matched well with the simulated pattern of crystal **I** obtained from *Mercury* (Fig. 2). The complete transformation of the starting components into the new solid phase of **I** was evidenced by the absence of the diffraction peaks at $2\theta = 9.4, 15.3, 18.6, 24.7$ and 26.5°

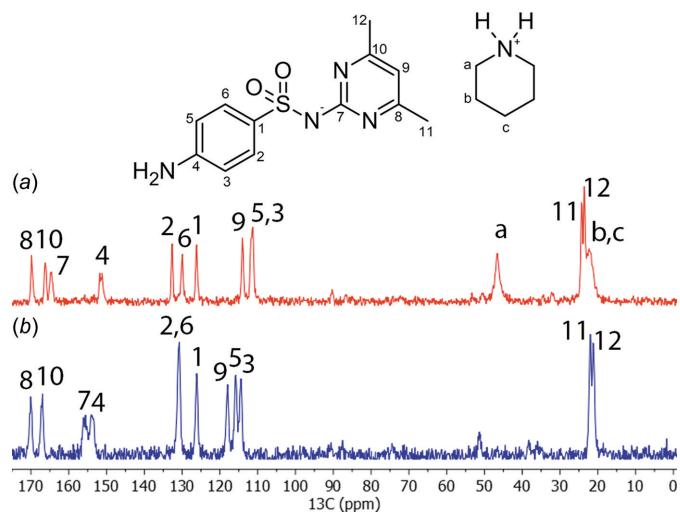


Figure 3
The solid-state ¹³C NMR spectra of (a) the polycrystalline powder of **I** and (b) SUL.

Table 2
CP/MAS solid-state ^{13}C NMR chemical shifts (ppm) of SUL and **I**.

	SUL	I		SUL	I
C1	126.1	126.1	C9	117.9	114.0
C2	130.8	132.6	C10	167.0	166.2
C3	114.4	111.2	C11	22.0	24.3
C4	153.9	151.1	C12	21.1	23.6
C5	115.8	111.2	C _a	–	21.9
C6	130.8	129.9	C _b	–	21.9
C7	155.9	164.6	C _c	–	46.6
C8	169.9	169.8			

belonging to the starting material SUL in the PXRD pattern of the polycrystalline powder of **I**, and the appearance of new diffraction peaks at $2\theta = 11.1, 12.2, 13.2, 14.5, 20.9, 22.0$ and 23.1° .

The polycrystalline powder of **I** was characterized by ^{13}C CP/MAS NMR spectroscopy and each signal represents a chemically different C atom. The ^{13}C NMR spectrum of SUL was assigned according to Fu *et al.* (2016) and Grossjohann *et al.* (2015), and was used to assign the spectrum of the polycrystalline powder of **I**. The ^{13}C NMR spectrum of **I** contained the signals for both SUL and PPD, and most of the ^{13}C NMR signals were shifted with respect to the ^{13}C NMR spectrum of SUL due to the change in the chemical environment as a consequence of the formation of the salt (Fig. 3). Evidence of the deprotonation of SUL was observed by the shift to a higher frequency of the C7 signal from 155.9 ppm in SUL to 164.6 ppm in **I** in a similar way to when SUL is deprotonated to form metallic complexes (Hossain *et al.*, 2007). A similar case is observed when saccharin is deprotonated to form salts with fluoroquinolones, since the ^{13}C NMR signal of the carbonyl C atom (next to the negatively charged N atom) is shifted from 164.0 to 172–173 ppm after deprotonation (Romañuk *et al.*, 2009). A comparison of the C7 chemical shifts, obtained from solid-state ^{13}C NMR spectroscopic analysis reported for cocrystals of SUL in the amidine form, and cocrystals and salts in the imine form (Fig. 4), revealed that in the amidine form, the C7 (C–NH) signal appeared at 155.2 ppm in the sulfamethazine–4-aminosalicylic acid cocrystal (similar to free SUL) (Grossjohann *et al.*, 2015), while in the sulfamethazine–saccharin cocrystal, where SUL adopts the imine form, the C7 (C=N) signal was shifted to a lower frequency, appearing at 152.7 ppm due to shielding caused by the formation of the C=N bond. In the sulfamethazinium

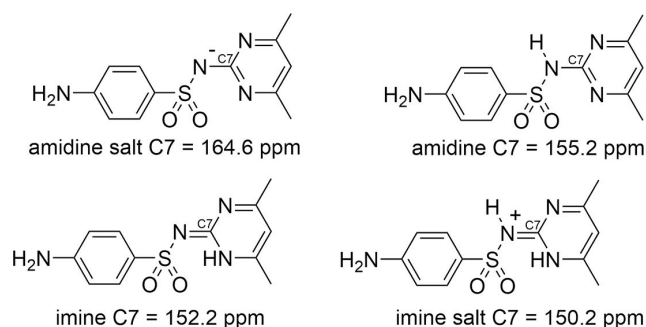


Figure 4
Chemical shift of the C7 ^{13}C NMR signal in the different forms of SUL.

Table 3
Hydrogen-bond geometry ($\text{\AA}, ^\circ$).

$D-H\cdots A$	$D-H$	$H\cdots A$	$D\cdots A$	$D-H\cdots A$
$\text{N1-H1D}\cdots\text{O1}^{\text{i}}$	0.88 (2)	2.06 (2)	2.9383 (18)	175.1 (17)
$\text{N1-H1E}\cdots\text{O1}^{\text{ii}}$	0.835 (19)	2.251 (19)	3.0397 (17)	157.6 (18)
$\text{N4-H4D}\cdots\text{O2}$	0.893 (18)	2.157 (18)	2.8980 (16)	140.0 (15)
$\text{N4-H4E}\cdots\text{N2}^{\text{iii}}$	0.951 (19)	1.865 (19)	2.8085 (18)	171.0 (15)

Symmetry codes: (i) $-x + \frac{3}{2}, y - \frac{1}{2}, -z + \frac{1}{2}$; (ii) $x + \frac{1}{2}, -y + \frac{1}{2}, z + \frac{1}{2}$; (iii) $-x + \frac{1}{2}, y - \frac{1}{2}, -z + \frac{1}{2}$.

saccharinate imine salt, the C7 signal (C=NH⁺) appeared at 150.2 ppm (shifted to a lower frequency), showing greater shielding due to the protonation of the C=N bond (Fu *et al.*, 2016) (Fig. 4). On the other hand, when amidine SUL is deprotonated as in **I**, the C7 (C–N[−]) signal appears at a higher frequency with respect to free SUL, because it is deshielded as a consequence of the negatively charged nitrogen effect. Whole assignments of the ^{13}C NMR signals are included in Table 2.

The thermal properties of the single crystal of **I** were investigated by TGA/DSC. The DSC plot of crystal **I** showed three endothermic peaks (Fig. 5). Considering that the crystal

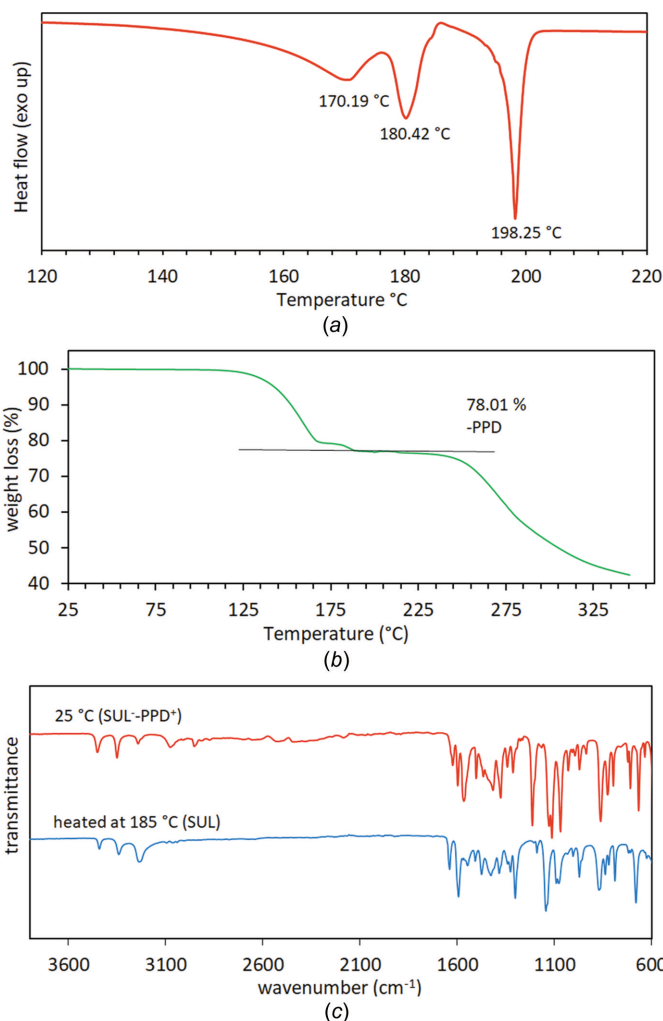


Figure 5
(a) The DSC curve of crystal **I**, (b) the TGA curve of crystal **I** and (c) the IR spectra of the polycrystalline powder of **I** before and after heating.

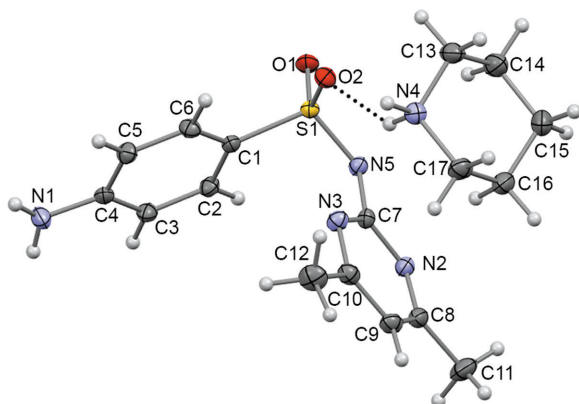


Figure 6
The asymmetric unit of **I**, showing the atom numbering. Displacement ellipsoids are drawn at the 50% probability level. Dashed lines represent hydrogen bonds.

structure of **I** is composed of only PPD and SUL, the peak at 170.19 °C is assigned to a solid–solid transition before the evaporation of PPD, the peak at 180.42 °C is assigned to the evaporation of PPD and the peak at 198.25 °C is attributed to the melting of SUL (Singh & Baruah, 2019). The TGA plot showed a weight loss of 21.99% at 185 °C, corresponding to the loss of PPD, as suggested by the DSC curve (Fig. 5). The mass loss after the melting of SUL is attributed to the degradation of SUL. To confirm the loss of PPD, a 100 mg

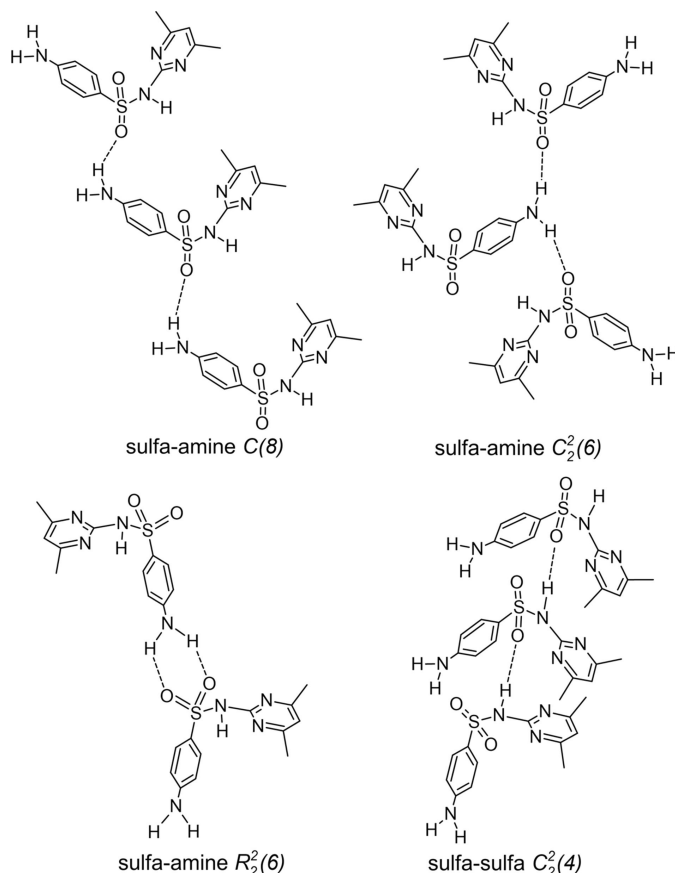


Figure 7
The hydrogen-bond patterns adopted in the self-assembly of SUL.

sample of the polycrystalline powder of **I** was heated at 185 °C for 1 h, then an IR spectrum was recorded and compared with that obtained at room temperature (25 °C). The IR spectrum of **I** obtained at 185 °C is similar to the IR spectrum of pure SUL, confirming the loss of PPD (Fig. 5).

3.2. Crystal structure of **I**

Salt **I** crystallized in the space group $P2_1/n$ with one SUL^- anion and one PPD^+ cation in the asymmetric unit ($Z = 4$) (Fig. 6) connected by an $\text{N}-\text{H}^+\cdots\text{O}=\text{S}$ ($\text{N4}-\text{H4D}\cdots\text{O2}$) hydrogen bond. The crystal structure of salt **I** showed deprotonation of the sulfonamide N atom of SUL and protonation of the amine group of PPD (to form the piperidinium group), as predicted by the ΔpK_a criteria. The SUL^- anion adopts a V shape, with a $\text{C1}-\text{S1}-\text{N5}-\text{C7}$ torsion angle of -61.39 (11)°. A search performed in the the CSD (accessed September 2022; Groom *et al.*, 2016) for crystal structures of pure SUL

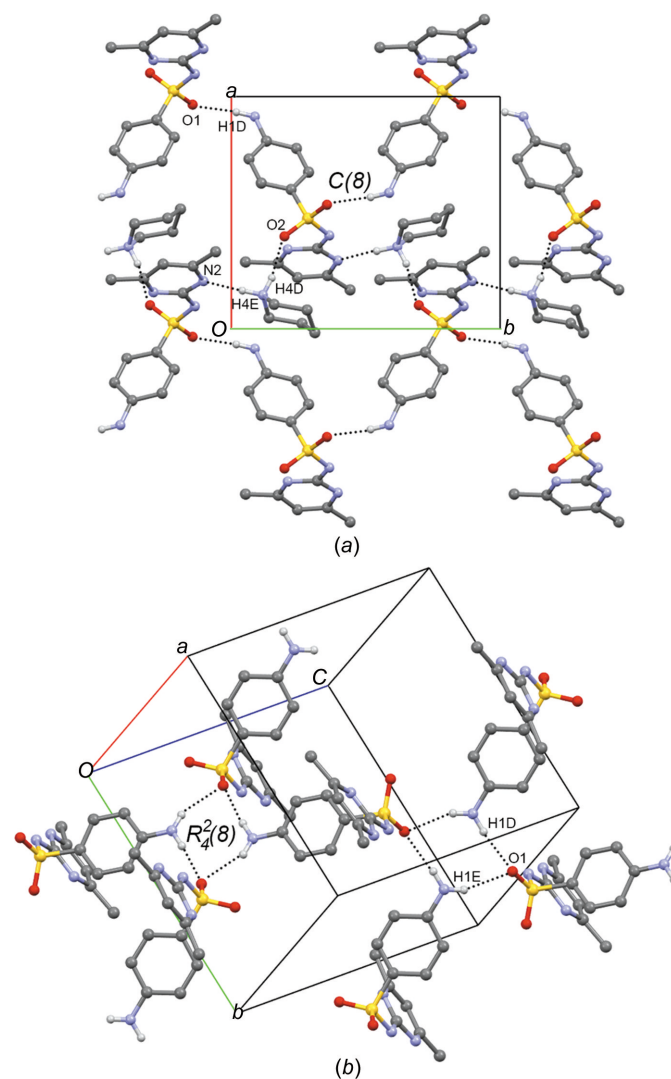


Figure 8
(a) The supramolecular sheet of **I** formed by interlinked $C(8)$ chains of SUL^- anions extended along the ab plane. (b) The interconnection of SUL^- anions depicting the $R_2^2(8)$ hydrogen-bond motif. Some H atoms have been omitted for clarity. Dashed lines represent hydrogen bonds.

and its cocrystals and salts in the amidine form, revealed that in the self-assembly of SUL molecules, four supramolecular patterns are preferred (three involving amine–sulfa interactions and one involving a sulfa–sulfa interaction) (Fig. 7). In salt **I**, the SUL^- anion adopts the sulfa–amine $C(8)$ pattern (Bernstein *et al.*, 1995) formed by the $\text{N1–H1D}\cdots\text{O1}^i$ hydrogen bond, producing a supramolecular tape running along the b axis. Hydrogen-bond details and symmetry codes of crystal **I** is given in Table 3. The two-dimensional supramolecular array is formed by the interlinking of $C(8)$ SUL^- tapes with the PPD^+ protons ($\text{N4–H4D}\cdots\text{O2}$ and $\text{N4–H4E}\cdots\text{N2}^{iii}$; Table 3), giving rise to a supramolecular sheet extended along the ab plane (Fig. 8). Supramolecular sheets are linked by $\text{N1–H1E}\cdots\text{O1}^{ii}$ and $\text{N1–H1D}\cdots\text{O1}^i$ hydrogen bonds involving two SUL^- anions and two PPD^+ cations, showing an $R_4^2(8)$ hydrogen-bond motif in a similar manner to the sulfamethazine–fumaric acid cocrystal (Fig. 8) (Ghosh *et al.*, 2011).

The crystal structure of pure SUL adopts the sulfa–sulfa $C_2^2(4)$ pattern (Fig. 7) and, after grinding, SUL transfers a proton to PPD (evidenced by the shift of the C7 signal in the ^{13}C CP/MAS NMR spectrum and the appearance of the band at 3067 cm^{-1} in the IR spectrum) to form the $\text{PPD}^+\cdot\text{SUL}^-$ salt, **I**, displaying the sulfa–amine $C(8)$ motif, changing the hydrogen-bonding pattern (evidenced by the shifts in the IR bands) and the chemical environment (shifting the ^{13}C NMR signals). Heating **I** at 185°C leads to the loss of PPD (according to DSC/TGA information and IR spectra) and the remaining SUL returns to the sulfa–sulfa $C_2^2(4)$ pattern before melting at 198.25°C .

4. Conclusions

The salt piperidinium sulfamethazine, $\text{PPD}^+\cdot\text{SUL}^-$, **I**, was obtained by solvent-assisted grinding. Proton transfer was confirmed by IR spectroscopy, solid-state ^{13}C NMR spectroscopy and single-crystal X-ray diffraction. The complete transformation of the starting material into the new crystalline phase was confirmed by PXRD analysis. The IR spectra and the PXRD patterns of the polycrystalline powder and the single crystal of **I** matched well, indicating a structural homogeneity between the polycrystalline powder and the single crystal. The crystal structure of salt $\text{PPD}^+\cdot\text{SUL}^-$ revealed a 1:1 stoichiometry and the SUL^- anion adopts the sulfa–amine $C(8)$ hydrogen-bond pattern, forming two-dimensional supramolecular sheets. Thermal analysis showed the loss of PPD before the melting of SUL.

Funding information

Funding for this research was provided by: Universidad de la Cañada (grant No. PFI-05/17); Facultad de Química, UNAM (grant No. PAIP 5000-9112).

References

- Agilent (2013). *CrysAlis PRO*. Agilent Technologies Ltd, Yarnton, Oxfordshire, England.
- Basak, A. K., Mazumdar, S. K. & Chaudhuri, S. (1983). *Acta Cryst.* **C39**, 492–494.
- Bernstein, J., Davis, R. E., Shimoni, L. & Chang, N. L. (1995). *Angew. Chem. Int. Ed. Engl.* **34**, 1555–1573.
- Bolla, G. & Nangia, A. (2016). *Chem. Commun.* **52**, 8342–8360.
- Caira, M. R. (2007). *Mol. Pharm.* **4**, 310–316.
- Farrugia, L. J. (2012). *J. Appl. Cryst.* **45**, 849–854.
- Fini, A., Cavallari, C., Bassini, G., Ospitali, F. & Morigi, R. (2012). *J. Pharm. Sci.* **101**, 3157–3168.
- Fu, X., Li, J., Wang, L., Wu, B., Xu, X., Deng, Z. & Zhang, H. (2016). *RSC Adv.* **6**, 26474–26478.
- Ghosh, S., Bag, P. P. & Reddy, C. M. (2011). *Cryst. Growth Des.* **11**, 3489–3503.
- Groom, C. R., Bruno, I. J., Lightfoot, M. P. & Ward, S. C. (2016). *Acta Cryst.* **B72**, 171–179.
- Grossjohann, C., Serrano, D. R., Paluch, K., O'Connell, P., Vella-Zarb, L., Manesiotis, P., McCabe, T., Tajber, L., Corrigan, O. I. & Healy, A. M. (2015). *J. Pharm. Sci.* **104**, 1385–1398.
- Güllüoğlu, M. T., Erdoğdu, Y. & Yurdakul, Ş. (2007). *J. Mol. Struct.* **834–836**, 540–547.
- Hossain, G. M. G., Amoroso, A. J., Banu, A. & Malik, K. M. A. (2007). *Polyhedron*, **26**, 967–974.
- Kamali, N., Aljohani, M., McArdle, P. & Erxleben, A. (2015). *Cryst. Growth Des.* **15**, 3905–3916.
- Kumar, S. & Nanda, A. (2018). *Mol. Cryst. Liq. Cryst.* **667**, 54–77.
- Luna, O. F., Gomez, J., Cárdenas, C., Albericio, F., Marshall, S. H. & Guzmán, F. (2016). *Molecules*, **21**, 1542.
- Macrae, C. F., Sovago, I., Cottrell, S. J., Galek, P. T. A., McCabe, P., Pidcock, E., Platings, M., Shields, G. P., Stevens, J. S., Towler, M. & Wood, P. A. (2020). *J. Appl. Cryst.* **53**, 226–235.
- Ovung, A. & Bhattacharyya, J. (2021). *Biophys. Rev.* **13**, 259–272.
- Pan, X., Zheng, Y., Chen, R., Qiu, S., Chen, Z., Rao, W., Chen, S., You, Y., Lü, J., Xu, L. & Guan, X. (2019). *Cryst. Growth Des.* **19**, 2455–2460.
- Pratt, J., Hutchinson, J. & Klein Stevens, C. L. (2011). *Acta Cryst.* **C67**, o487–o491.
- Romañuk, C. B., Manzo, R. H., Linck, Y. G., Chattah, A. K., Monti, G. A. & Olivera, M. E. (2009). *J. Pharm. Sci.* **98**, 3788–3801.
- Sanphui, P. & Bolla, G. (2018). *Cryst. Growth Des.* **18**, 5690–5711.
- Serrano, D. R., Persoons, T., D'Arcy, D. M., Galiana, C., Dea-Ayuela, M. A. & Healy, A. M. (2016). *Eur. J. Pharm. Sci.* **89**, 125–136.
- Sheldrick, G. M. (2015a). *Acta Cryst.* **A71**, 3–8.
- Sheldrick, G. M. (2015b). *Acta Cryst.* **C71**, 3–8.
- Silverstein, R. M., Bassler, G. C. & Morrill, T. C. (1991). *Spectrometric Identification of Organic Compounds*, 5th ed., p. 103. New York: Wiley.
- Singh, M. P. & Baruah, J. B. (2019). *ACS Omega*, **4**, 11609–11620.
- Taylor, S. M. & Patel, U. H. (2015). *J. Coord. Chem.* **68**, 2192–2207.
- Yang, X. L., Liu, J., Yang, L. & Zhang, X. Y. (2005). *Synth. React. Inorg. Met.-Org. Nano-Met. Chem.* **35**, 761–766.
- Zhang, C., Lai, C., Zeng, G., Huang, D., Yang, C., Wang, Y., Zhou, Y. & Cheng, M. (2016). *Water Res.* **95**, 103–112.
- Zhang, X., Zhou, L., Wang, C., Li, Y., Wu, Y., Zhang, M. & Yin, Q. (2017). *Cryst. Growth Des.* **17**, 6151–6157.

supporting information

Acta Cryst. (2023). C79, 71-76 [https://doi.org/10.1107/S2053229622012050]

Crystal structure and characterization of the sulfamethazine–piperidine salt

Juan Saulo González-González, Salvador Pérez-Espinoza, Francisco Javier Martínez-Martínez, Armando Pineda-Contreras, Miguel Ángel Canseco-Martínez, Marcos Flores-Alamo and Héctor García-Ortega

Computing details

Data collection: *CrysAlis PRO* (Agilent, 2013); cell refinement: *CrysAlis PRO* (Agilent, 2013); data reduction: *CrysAlis PRO* (Agilent, 2013); program(s) used to solve structure: SHELXT2018 (Sheldrick, 2015a)¹; program(s) used to refine structure: SHELXL2018 (Sheldrick, 2015b)²; molecular graphics: *ORTEP* for Windows (Farrugia, 2012); software used to prepare material for publication: *ORTEP* for Windows (Farrugia, 2012).

Piperidin-1-ium 4-[[4,6-dimethylpyrimidin-2-yl)azanidyl]sulfonyl]aniline

Crystal data

$C_5H_{12}N^+ \cdot C_{12}H_{13}N_4O_2S^-$
 $M_r = 363.48$
 Monoclinic, $P2_1/n$
 Hall symbol: -P 2yn
 $a = 10.5713$ (7) Å
 $b = 12.1313$ (8) Å
 $c = 14.3623$ (10) Å
 $\beta = 97.182$ (7)°
 $V = 1827.4$ (2) Å³
 $Z = 4$

$F(000) = 776$
 $D_x = 1.321$ Mg m⁻³
 Mo $K\alpha$ radiation, $\lambda = 0.71073$ Å
 Cell parameters from 4261 reflections
 $\theta = 3.7$ – 29.4 °
 $\mu = 0.20$ mm⁻¹
 $T = 130$ K
 Prism, colourless
 $0.53 \times 0.43 \times 0.34$ mm

Data collection

Agilent Xcalibur Atlas Gemini
 diffractometer
 Graphite monochromator
 Detector resolution: 10.4685 pixels mm⁻¹
 ω scans
 Absorption correction: analytical
 (CrysAlis PRO; Agilent, 2013)
 $T_{\min} = 0.93$, $T_{\max} = 0.945$

10086 measured reflections
 4298 independent reflections
 3667 reflections with $I > 2\sigma(I)$
 $R_{\text{int}} = 0.025$
 $\theta_{\max} = 29.4$ °, $\theta_{\min} = 3.9$ °
 $h = -14 \rightarrow 10$
 $k = -15 \rightarrow 15$
 $l = -19 \rightarrow 19$

Refinement

Refinement on F^2
 Least-squares matrix: full
 $R[F^2 > 2\sigma(F^2)] = 0.037$
 $wR(F^2) = 0.102$
 $S = 1.04$
 4298 reflections
 241 parameters
 0 restraints

Hydrogen site location: mixed
 H atoms treated by a mixture of independent
 and constrained refinement
 $w = 1/[\sigma^2(F_o^2) + (0.0483P)^2 + 0.7985P]$
 where $P = (F_o^2 + 2F_c^2)/3$
 $(\Delta/\sigma)_{\max} < 0.001$
 $\Delta\rho_{\max} = 0.37$ e Å⁻³
 $\Delta\rho_{\min} = -0.43$ e Å⁻³

Extinction correction: SHELXL2018
 (Sheldrick, 2015b),
 $F_c^* = k F_c [1 + 0.001 x F_c^2 \lambda^3 / \sin(2\theta)]^{-1/4}$
 Extinction coefficient: 0.0340 (19)

Special details

Geometry. All esds (except the esd in the dihedral angle between two l.s. planes) are estimated using the full covariance matrix. The cell esds are taken into account individually in the estimation of esds in distances, angles and torsion angles; correlations between esds in cell parameters are only used when they are defined by crystal symmetry. An approximate (isotropic) treatment of cell esds is used for estimating esds involving l.s. planes.

Refinement. Structure solution and refinement were carried out with the programs SHELXT (Sheldrick, 2015a) and SHELXL (Sheldrick, 2015b). Full-matrix least-squares refinement was carried out by minimizing $(F_o^2 - F_c^2)^2$. All nonhydrogen atoms were refined anisotropically.

Fractional atomic coordinates and isotropic or equivalent isotropic displacement parameters (\AA^2)

	<i>x</i>	<i>y</i>	<i>z</i>	U_{iso}^*/U_{eq}
C1	0.60035 (12)	0.22230 (11)	0.25758 (9)	0.0157 (3)
C2	0.67492 (13)	0.28748 (11)	0.32312 (9)	0.0182 (3)
H2	0.65524	0.363375	0.329028	0.022*
C3	0.77718 (13)	0.24215 (12)	0.37940 (9)	0.0197 (3)
H3	0.82675	0.286949	0.424364	0.024*
C4	0.80861 (13)	0.13058 (12)	0.37083 (9)	0.0181 (3)
C5	0.73159 (14)	0.06562 (12)	0.30567 (10)	0.0202 (3)
H5	0.750755	-0.010311	0.299307	0.024*
C6	0.62780 (13)	0.11129 (12)	0.25051 (9)	0.0186 (3)
H6	0.57522	0.066153	0.207624	0.022*
C7	0.34585 (12)	0.32016 (11)	0.31808 (9)	0.0162 (3)
C8	0.22968 (13)	0.35756 (13)	0.43981 (10)	0.0207 (3)
C9	0.22099 (13)	0.24615 (13)	0.45791 (10)	0.0218 (3)
H9	0.174167	0.219714	0.505634	0.026*
C10	0.28327 (13)	0.17430 (13)	0.40372 (10)	0.0206 (3)
C11	0.16802 (17)	0.44169 (15)	0.49643 (11)	0.0319 (4)
H11A	0.096558	0.407673	0.523126	0.048*
H11B	0.136598	0.503284	0.455826	0.048*
H11C	0.230717	0.468944	0.547253	0.048*
C12	0.28810 (16)	0.05272 (13)	0.42176 (12)	0.0293 (4)
H12A	0.375567	0.031146	0.445425	0.044*
H12B	0.260541	0.013203	0.363215	0.044*
H12C	0.231349	0.034225	0.468445	0.044*
C13	0.10554 (16)	0.15893 (13)	0.06282 (10)	0.0260 (3)
H13A	0.026839	0.120407	0.03583	0.031*
H13B	0.172866	0.143158	0.022577	0.031*
C14	0.08120 (17)	0.28175 (14)	0.06426 (11)	0.0302 (4)
H14A	0.049704	0.307106	0.000019	0.036*
H14B	0.162193	0.32063	0.084921	0.036*
C15	-0.01636 (15)	0.31071 (15)	0.13004 (11)	0.0294 (4)
H15A	-0.023773	0.391834	0.13455	0.035*
H15B	-0.100831	0.281017	0.104464	0.035*

C16	0.02347 (15)	0.26287 (14)	0.22704 (10)	0.0264 (3)
H16A	0.101906	0.300294	0.25596	0.032*
H16B	-0.044486	0.276703	0.267176	0.032*
C17	0.04779 (15)	0.14019 (14)	0.22257 (11)	0.0258 (3)
H17A	0.077358	0.11204	0.286279	0.031*
H17B	-0.032413	0.101686	0.198981	0.031*
N1	0.91410 (13)	0.08717 (12)	0.42253 (9)	0.0247 (3)
H1D	0.9330 (18)	0.0180 (17)	0.4128 (13)	0.03*
H1E	0.9426 (18)	0.1211 (16)	0.4712 (13)	0.03*
N2	0.29435 (11)	0.39582 (10)	0.37202 (8)	0.0184 (3)
N3	0.34236 (11)	0.21007 (10)	0.33225 (8)	0.0189 (3)
N4	0.14602 (12)	0.11727 (11)	0.15932 (8)	0.0193 (3)
H4D	0.2191 (17)	0.1505 (15)	0.1814 (12)	0.023*
H4E	0.1647 (16)	0.0409 (16)	0.1552 (12)	0.023*
N5	0.40244 (11)	0.36429 (10)	0.24673 (8)	0.0171 (2)
O1	0.53436 (9)	0.35578 (9)	0.12003 (7)	0.0208 (2)
O2	0.39831 (9)	0.19763 (8)	0.13606 (7)	0.0210 (2)
S1	0.47516 (3)	0.28499 (3)	0.18398 (2)	0.01499 (11)

Atomic displacement parameters (Å²)

	U^{11}	U^{22}	U^{33}	U^{12}	U^{13}	U^{23}
C1	0.0145 (6)	0.0194 (7)	0.0136 (6)	0.0011 (5)	0.0033 (5)	0.0008 (5)
C2	0.0187 (6)	0.0172 (7)	0.0190 (6)	0.0011 (5)	0.0037 (5)	-0.0033 (5)
C3	0.0177 (6)	0.0235 (7)	0.0174 (6)	0.0004 (6)	0.0011 (5)	-0.0052 (6)
C4	0.0174 (6)	0.0242 (7)	0.0133 (6)	0.0023 (6)	0.0040 (5)	0.0021 (5)
C5	0.0236 (7)	0.0165 (7)	0.0204 (6)	0.0032 (6)	0.0029 (6)	-0.0003 (5)
C6	0.0204 (6)	0.0181 (7)	0.0169 (6)	-0.0013 (5)	0.0009 (5)	-0.0024 (5)
C7	0.0132 (6)	0.0180 (6)	0.0173 (6)	0.0013 (5)	0.0016 (5)	0.0004 (5)
C8	0.0171 (6)	0.0281 (8)	0.0169 (6)	0.0016 (6)	0.0030 (5)	-0.0011 (6)
C9	0.0195 (7)	0.0289 (8)	0.0177 (6)	-0.0030 (6)	0.0050 (5)	0.0028 (6)
C10	0.0192 (7)	0.0227 (7)	0.0197 (6)	-0.0025 (6)	0.0015 (5)	0.0034 (6)
C11	0.0355 (9)	0.0340 (9)	0.0294 (8)	0.0050 (7)	0.0166 (7)	-0.0025 (7)
C12	0.0358 (9)	0.0225 (8)	0.0308 (8)	-0.0035 (7)	0.0084 (7)	0.0068 (7)
C13	0.0318 (8)	0.0285 (8)	0.0181 (6)	0.0017 (7)	0.0043 (6)	-0.0007 (6)
C14	0.0371 (9)	0.0297 (9)	0.0244 (7)	0.0091 (7)	0.0069 (7)	0.0055 (6)
C15	0.0236 (7)	0.0357 (9)	0.0283 (8)	0.0084 (7)	0.0010 (6)	-0.0010 (7)
C16	0.0231 (7)	0.0335 (9)	0.0232 (7)	0.0034 (7)	0.0052 (6)	-0.0040 (7)
C17	0.0236 (7)	0.0333 (9)	0.0219 (7)	-0.0025 (6)	0.0083 (6)	0.0011 (6)
N1	0.0245 (6)	0.0269 (7)	0.0210 (6)	0.0074 (5)	-0.0038 (5)	-0.0020 (5)
N2	0.0175 (5)	0.0192 (6)	0.0189 (5)	0.0019 (5)	0.0039 (5)	0.0001 (5)
N3	0.0195 (6)	0.0176 (6)	0.0204 (5)	-0.0003 (5)	0.0057 (5)	0.0014 (5)
N4	0.0187 (6)	0.0190 (6)	0.0203 (6)	-0.0033 (5)	0.0027 (5)	-0.0008 (5)
N5	0.0177 (5)	0.0164 (6)	0.0178 (5)	0.0025 (4)	0.0049 (4)	0.0018 (4)
O1	0.0222 (5)	0.0247 (5)	0.0163 (4)	-0.0002 (4)	0.0057 (4)	0.0045 (4)
O2	0.0193 (5)	0.0237 (5)	0.0193 (5)	-0.0016 (4)	-0.0008 (4)	-0.0033 (4)
S1	0.01488 (17)	0.01668 (18)	0.01356 (16)	0.00063 (12)	0.00244 (12)	0.00128 (12)

Geometric parameters (Å, °)

C1—C6	1.3840 (19)	C12—H12B	0.98
C1—C2	1.3954 (18)	C12—H12C	0.98
C1—S1	1.7600 (13)	C13—N4	1.4870 (19)
C2—C3	1.3806 (19)	C13—C14	1.513 (2)
C2—H2	0.95	C13—H13A	0.99
C3—C4	1.403 (2)	C13—H13B	0.99
C3—H3	0.95	C14—C15	1.524 (2)
C4—N1	1.3657 (18)	C14—H14A	0.99
C4—C5	1.403 (2)	C14—H14B	0.99
C5—C6	1.3860 (19)	C15—C16	1.519 (2)
C5—H5	0.95	C15—H15A	0.99
C6—H6	0.95	C15—H15B	0.99
C7—N3	1.3522 (18)	C16—C17	1.513 (2)
C7—N2	1.3581 (18)	C16—H16A	0.99
C7—N5	1.3594 (17)	C16—H16B	0.99
C8—N2	1.3406 (18)	C17—N4	1.4888 (19)
C8—C9	1.382 (2)	C17—H17A	0.99
C8—C11	1.503 (2)	C17—H17B	0.99
C9—C10	1.388 (2)	N1—H1D	0.88 (2)
C9—H9	0.95	N1—H1E	0.835 (19)
C10—N3	1.3388 (18)	N4—H4D	0.893 (18)
C10—C12	1.497 (2)	N4—H4E	0.951 (19)
C11—H11A	0.98	N5—S1	1.5817 (12)
C11—H11B	0.98	O1—S1	1.4548 (10)
C11—H11C	0.98	O2—S1	1.4551 (10)
C12—H12A	0.98		
C6—C1—C2	119.67 (12)	N4—C13—H13B	109.5
C6—C1—S1	121.68 (10)	C14—C13—H13B	109.5
C2—C1—S1	118.63 (11)	H13A—C13—H13B	108.1
C3—C2—C1	120.27 (13)	C13—C14—C15	111.41 (14)
C3—C2—H2	119.9	C13—C14—H14A	109.3
C1—C2—H2	119.9	C15—C14—H14A	109.3
C2—C3—C4	120.65 (13)	C13—C14—H14B	109.3
C2—C3—H3	119.7	C15—C14—H14B	109.3
C4—C3—H3	119.7	H14A—C14—H14B	108
N1—C4—C3	120.71 (13)	C16—C15—C14	110.42 (13)
N1—C4—C5	120.82 (14)	C16—C15—H15A	109.6
C3—C4—C5	118.44 (12)	C14—C15—H15A	109.6
C6—C5—C4	120.57 (13)	C16—C15—H15B	109.6
C6—C5—H5	119.7	C14—C15—H15B	109.6
C4—C5—H5	119.7	H15A—C15—H15B	108.1
C1—C6—C5	120.35 (13)	C17—C16—C15	111.47 (13)
C1—C6—H6	119.8	C17—C16—H16A	109.3
C5—C6—H6	119.8	C15—C16—H16A	109.3
N3—C7—N2	124.15 (12)	C17—C16—H16B	109.3

N3—C7—N5	121.69 (12)	C15—C16—H16B	109.3
N2—C7—N5	114.17 (12)	H16A—C16—H16B	108
N2—C8—C9	121.82 (13)	N4—C17—C16	110.17 (12)
N2—C8—C11	116.92 (14)	N4—C17—H17A	109.6
C9—C8—C11	121.25 (13)	C16—C17—H17A	109.6
C8—C9—C10	117.48 (13)	N4—C17—H17B	109.6
C8—C9—H9	121.3	C16—C17—H17B	109.6
C10—C9—H9	121.3	H17A—C17—H17B	108.1
N3—C10—C9	121.72 (14)	C4—N1—H1D	117.9 (12)
N3—C10—C12	116.29 (13)	C4—N1—H1E	116.8 (13)
C9—C10—C12	122.00 (14)	H1D—N1—H1E	122.6 (18)
C8—C11—H11A	109.5	C8—N2—C7	117.23 (12)
C8—C11—H11B	109.5	C10—N3—C7	117.36 (12)
H11A—C11—H11B	109.5	C13—N4—C17	111.33 (12)
C8—C11—H11C	109.5	C13—N4—H4D	108.2 (11)
H11A—C11—H11C	109.5	C17—N4—H4D	109.7 (11)
H11B—C11—H11C	109.5	C13—N4—H4E	108.2 (10)
C10—C12—H12A	109.5	C17—N4—H4E	112.7 (10)
C10—C12—H12B	109.5	H4D—N4—H4E	106.5 (15)
H12A—C12—H12B	109.5	C7—N5—S1	118.76 (10)
C10—C12—H12C	109.5	O1—S1—O2	112.96 (6)
H12A—C12—H12C	109.5	O1—S1—N5	106.19 (6)
H12B—C12—H12C	109.5	O2—S1—N5	115.47 (6)
N4—C13—C14	110.59 (12)	O1—S1—C1	106.49 (6)
N4—C13—H13A	109.5	O2—S1—C1	107.62 (6)
C14—C13—H13A	109.5	N5—S1—C1	107.65 (6)
C6—C1—C2—C3	1.3 (2)	N3—C7—N2—C8	-4.15 (19)
S1—C1—C2—C3	-177.34 (10)	N5—C7—N2—C8	175.69 (11)
C1—C2—C3—C4	0.8 (2)	C9—C10—N3—C7	3.89 (19)
C2—C3—C4—N1	176.12 (13)	C12—C10—N3—C7	-176.15 (13)
C2—C3—C4—C5	-1.8 (2)	N2—C7—N3—C10	0.54 (19)
N1—C4—C5—C6	-177.21 (13)	N5—C7—N3—C10	-179.28 (12)
C3—C4—C5—C6	0.7 (2)	C14—C13—N4—C17	58.69 (17)
C2—C1—C6—C5	-2.4 (2)	C16—C17—N4—C13	-58.96 (16)
S1—C1—C6—C5	176.21 (11)	N3—C7—N5—S1	-4.87 (17)
C4—C5—C6—C1	1.4 (2)	N2—C7—N5—S1	175.29 (9)
N2—C8—C9—C10	0.7 (2)	C7—N5—S1—O1	-175.12 (10)
C11—C8—C9—C10	-178.52 (13)	C7—N5—S1—O2	58.85 (12)
C8—C9—C10—N3	-4.5 (2)	C7—N5—S1—C1	-61.39 (11)
C8—C9—C10—C12	175.53 (14)	C6—C1—S1—O1	-109.20 (12)
N4—C13—C14—C15	-55.83 (18)	C2—C1—S1—O1	69.41 (12)
C13—C14—C15—C16	53.48 (19)	C6—C1—S1—O2	12.19 (13)
C14—C15—C16—C17	-54.01 (18)	C2—C1—S1—O2	-169.20 (10)
C15—C16—C17—N4	56.68 (17)	C6—C1—S1—N5	137.27 (12)
C9—C8—N2—C7	3.38 (19)	C2—C1—S1—N5	-44.12 (12)
C11—C8—N2—C7	-177.37 (12)		

Hydrogen-bond geometry (Å, °)

<i>D</i> —H··· <i>A</i>	<i>D</i> —H	H··· <i>A</i>	<i>D</i> ··· <i>A</i>	<i>D</i> —H··· <i>A</i>
C9—H9···O1 ⁱ	0.95	2.52	3.4629 (18)	175
N1—H1D···O1 ⁱⁱ	0.88 (2)	2.06 (2)	2.9383 (18)	175.1 (17)
N1—H1E···O1 ⁱⁱⁱ	0.835 (19)	2.251 (19)	3.0397 (17)	157.6 (18)
N4—H4D···N3	0.893 (18)	2.492 (18)	3.2334 (17)	140.8 (14)
N4—H4D···O2	0.893 (18)	2.157 (18)	2.8980 (16)	140.0 (15)
N4—H4E···N2 ^{iv}	0.951 (19)	1.865 (19)	2.8085 (18)	171.0 (15)
N4—H4E···N5 ^{iv}	0.951 (19)	2.706 (18)	3.4168 (17)	132.0 (13)

Symmetry codes: (i) $x-1/2, -y+1/2, z+1/2$; (ii) $-x+3/2, y-1/2, -z+1/2$; (iii) $x+1/2, -y+1/2, z+1/2$; (iv) $-x+1/2, y-1/2, -z+1/2$.